A MINIATURE HIGH-SENSITIVITY BROAD-BAND ACCELEROMETER BASED ON ELECTRON TUNNELING TRANSDUCERS

Howard K. Rockstad, T. W. Kenny, J. K. Reynolds, and W. J. Kaiser
Jet Propulsion Laboratory
Center for Space Microelectronics Technology
California Institute of Technology
Pasadena, California 91109-8099 (U. S.A.)

Thomas B. Gabrielson
Naval Air Warfare Center, Code 5044
Warminster, Pennsylvania 18974-0591 (U. S.A.)

ABSTRACT

New high-sensitivity microsensors have been developed using high-resolution position sensors based on electron tunneling. Design of miniature accelerometers having resolutions approaching 10-9 $g/\sqrt{Hz}$ is discussed. A new dual-element electron tunneling structure, which overcomes bandwidth limitations of single-element structures, allows design of high sensitivity accelerometers operating in a band from a few Hz to several kHz. A miniature accelerometer based on this structure can thus have application as a sensitive acoustic sensor. Thermal vibration of the, proof mass is an extremely important constraint in miniature accelerometers, and can be the dominant limitation on the sensitivity. Thermal noise is analyzed for the suspended masses of the dual-element structure, and compared with electronic noise in the tunneling circuit. With a proof mass

of 100 mg, noise analysis predicts limiting resolutions approaching 10-9 $g/\sqrt{Hz}$ in a 300 Hz band and 10-8 $g/\sqrt{Hz}$ at 1 kHz. Prototype accelerometers have been fabricated by silicon micromachining and tested. A noise resolution of 10-7 $g/\sqrt{Hz}$ between 4 and 70 Hz and 6 x 10-7 $g/\sqrt{Hz}$ at 400 Hz is observed in a damped device. The low-frequency responsivity of this device is 100,000 V/g, decreasing to 1300 V/g at 600 Hz.

INTRODUCTION

Displacement transducers based on electron tunneling have been proposed for use in a wide variety of physical sensors. These sensors utilize the high position sensitivity of electron tunneling. Displacement resolutions approaching 10-4 $Å/\sqrt{Hz}$ have been shown by Waltman and Kaiser[1] and by Kenny, *et al.*[2] for tunnel transducers. Employing a gold tip formed by breaking a gold wire, and a piezoelectric bimorph as both the proof mass and the control element of the system, Waltman and Kaiser observed an acceleration resolution of 10-5 $g/\sqrt{Hz}$ with a bandwidth of 3 kHz. Baski, *et al.* [3] utilized a beryllium-. copper spring and a 2 gram proof mass mounted within a miniature Scanning Tunneling Microscope (STM) with a tungsten tip and a graphite counter electrode to measure acceleration resolution better than 10-4 $g/\sqrt{Hz}$ in a 200 Hz band.

Recent work has focused on the development of tunneling accelerometers based on silicon micromachining. Kenny, *et al.*[2] demonstrated an operational tunneling accelerometer which featured a micromachined folded-cantilever proof mass suspension and a gold-coated silicon tip. Control of the position of the cantilever was accomplished via electrostatic deflection. During operation of this device, acceleration forces on the cantilever are balanced by electrostatic forces generated by a feedback circuit, so as to keep the cantilever in the same relative position with respect to the frame. The bandwidth of the feedback circuit is limited to less than the mechanical resonance frequency of 200

Hz in order to prevent oscillation. An acceleration resolution of 10-7 $g/\sqrt{Hz}$ at 10 Hz is inferred from noise measurements.[4]

MacDonald and co-workers have developed a series of high-resolution silicon microfabrication techniques for use in construction of two-dimensional scanning/tunneling structures.[5] These devices achieve very high resonant frequencies and a capability for integration of electronics on the microstructure through use of lateral oxidation and etching to release single crystal micromechanical elements from the substrate. Kobayashi, *et al.* [6] *have* demonstrated a surface-micromachined lateral tunneling unit, which is fabricated by deposition of sacrificial layers and polysilicon, with subsequent patterning, etching, and metallization. Tunneling currents were observed, but with weaker than expected variation with applied actuator voltage, indicating the possibility of adsorbates or other contaminants on the gold electrode surfaces. Zavracky and co-workers have also recently started an effort to fabricate a bulk-micromachined tunneling accelerometer for microgravity studies.7"

Other tunnel sensor development activities include a magnetometer based on detection of the magnetostriction of a metglas ribbon,[8,9] an infrared sensor based on detection of expansion of a heated volume of trapped gas, [10] and a tactile sensor based on use of a tunneling or field-emitting transducer to detect deflection of a flexible surface structure. [11] Studies of the fundamental limits to the performance of tunneling transducers are also being carried out.[12,13]

In all these sensor development activities, it has become clear that the successful operation of the tunnel sensor requires certain fundamental characteristics. Most important is the cleanliness of the metallic tunneling electrodes. Since the sensor components are exposed to air at some time during assembly or operation, it is important that the metal chosen for the electrodes be resistant to oxidation or other contamination, In all of the work conducted in our group, gold electrodes are utilized because of gold's resistance to contamination in air. It is also important to consider the possibility of

migration of subsurface species to the surface of gold, where oxidation would occur. For example, silicon is known to migrate through gold films to the surface, where a non-conducting Si02 layer is formed. To prevent this phenomenon, it is important to passivate the silicon surface with a non-migrating coating, such as Si02 or Si3N4, before application of the gold film. Also, it is important to choose materials for the adhesion and diffusion barrier layer between the gold and the substrate which will not migrate through to the surface of the gold. If the gold film needs to be patterned, evaporation through a shadow mask in UHV is preferable. Alternatively, it is possible to pattern gold films by lift-off techniques, but post-process cleaning is required to remove organic residue.

As a result of development, we have concluded that the shape of the tunneling tip is relatively unimportant for the operation of the device. We have utilized microfabricated tips with radii of curvature less than 1 micron, as well as microfabricated tips which have flat ends (radii > 100 microns) with no difference in performance. On a recent version of the accelerometer, the tip was eliminated entirely in favor of a tunneling geometry which featured a triangular cantilever and a flat counter-electrode. Presumably, tunneling occurred at some point along the edge of the cantilever in this device. The reason for this insensitivity to tip shape lies in the steep exponential dependence between tunneling current and separation between clean metal electrodes. Because of this steep dependence, any pair of surfaces will first approach one another between a single pair of atoms, and this pair will dominate the tunneling current. Because of this situation, we no longer include sophisticated and time-consuming tip-sharpening processes in the tunnel sensor fabrication sequence. On the contrary, the tips for the tunneling infrared sensor are smoothed to reduce the possibility of perforation of the counter electrode.

Finally, we have had the best operational success with tunneling sensors which are based on feedback control of wide-bandwidth mechanical elements, The inclusion of wide-bandwidth actuators allows utilization of simple, easily operated, wide-bandwidth feedback circuitry with very high gain over a band of frequencies. In such a situation, the

feedback circuit is able to control the separation between the tunneling electrodes to much better than a fraction of an Angstrom. This level of control insures the retention of continuous tunneling, rather than intermittent tunneling caused by intermittent electrode separation, which can be a cause of sensor failure. In addition, the continuous retention of tunneling current is required to achieve the high sensitivity to displacement that makes tunneling transducers desirable.

Operation of a tunnel tip in an STM mode is illustrated in Ref. 2. A tunnel current I is established between a tip and a counterelectrode by a small bias voltage V. In typical STM operation, feedback circuitry controls the vertical position of the tip by means of a piezoelectric transducer so as to maintain the tunnel current constant, thereby also maintaining the electrode spacings constant, while the specimen is scanned laterally. Tunnel current I depends on electrode spacings as [14]

$$I \propto Ve^{-\alpha\sqrt{\Phi}s} \tag{1}$$

where a = 1.025 $Å^{-1}eV^{-1/2}$, Φ is the height of the tunnel barrier, and the bias voltage V (typically about 200 mV) is small compared to Φ. For typical values of@ and s (0.5 eV and 10 Å, respectively), the current varies by a factor of two for each Å change in, electrode separation. Because of this extreme sensitivity to position, the tip-to-substrate separation is maintained constant to high precision, The tunnel transducer's sensitivity to position is superior to that of other compact transducers, such as standard compact capacitive sensors. The sensitivity of a tunnel transducer is independent of device size, because of the extremely small size of the tunneling tip, in contrast with a capacitive sensor, for example. Thus, miniaturization of the transducer causes no direct reduction in sensitivity.

Miniature accelerometers have been described by numerous authors. [15-20] Some miniature accelerometers are intended for fairly large forces, such as those encountered in automotive applications for air bag deployment. Other applications require sensitivity

to extremely, small signals, and in this regime Rudolf [1]8 has described a capacitive accelerometer with micro-g resolution at 1 Hz.

Sensitive compact accelerometers capable of detecting accelerations of the order of 10-7 to 10-9 $g/\sqrt{Hz}$ in a band from several Hz to several kHz are the subject of this paper. Such accelerometers can have application as sensitive acoustic sensors. Growing needs for small, low-cost accelerometers include network applications using an array of distributed units. Accelerometers function by employing proof masses whose motion responds to accelerations. Motion of the proof mass relative to the accelerometer case is measured directly; the motion of the case is determined from the motion of the mass and knowledge of the sensor dynamic response. Achievement of very high resolution requires novel approaches, such as that of the electron tunneling transducer described above, for measuring displacement of the proof mass relative to the case. In this paper, a new tunnel accelerometer designed to achieve high resolution over a broad band of several kHz is described. High resolution in a miniature micromachined-silicon sensor is achieved by use of an electron tunneling transducer. Broadband operation is achieved by use of an innovative dual-cantilever structure.

DUAL-ELEMENT TUNNEL ACCELEROMETER

The tunnel accelerometer described by Kenny, et al.[2] comprises a single suspended mass component, the proof mass. Electron tunneling takes place between a tip on the proof mass and a fixed counter electrode on the case. Operation of this accelerometer uses electronic feedback circuitry to maintain a constant tip-to-counter electrode spacing, as in scanning tunneling microscopy, by,. controlling an electrostatic deflection voltage on the suspended mass. When the sensor is accelerated, the proof mass experiences an inertial force which causes it's motion to lag that of the sensor. The feedback circuit generates an electrostatic re-balance force which causes the proof mass

to follow the motion of the sensor. In order to achieve stable operation, the bandwidth of the feedback circuit is restricted to frequencies below the natural frequency of the proof mass, 200 Hz in this case.

Many applications require a larger bandwidth. To overcome the frequency limitations of the single-element system, a new dual-element system has been designed, as illustrated in Fig. 1. This design separates the proof mass and the electrical transducer so that their mechanical properties can be independently tailored. Tunneling occurs between electrodes on a wide-bandwidth cantilever and on the proof mass. The wide-bandwidth cantilever is controlled electrostatically by high-frequency feedback circuitry to closely follow the motion of the proof mass. Since the proof mass may have a low resonant frequency, it's dynamics may be tuned to enhance acceleration sensitivity. An optional low-frequency secondary feedback circuit maintains the mass position within suitable range of the cantilever. The output signal of the transducer is derived from the high-frequency feedback circuitry, as illustrated in Fig. 2, This signal has bandwidth > 10 kHz, and the dynamic range above the noise floor of the transducer is > 100 dB.

THEORY

Performance of a sensor system depends on noise sources inherent within the system as well as on the responsivity of the system. As has been described by Gabrielson[21] and is shown in the following analysis, thermal vibration of the proof mass is an extremely important consideration for a high-sensitivity miniature accelerometer. Noise sources are analyzed here for a dual-element design, represented by the mass-suspension system in Fig. 3. The proof mass m_p and cantilever mass m_c are suspended independently from the case with spring constants k_p and kc, and with damping coefficients R_p and R_c. The relations between the mass motions and the case motion can be obtained by solving the equations of motion when the case is subjected to a sinusoidal

driving force. From the steady-state solutions for each mass, the relations between the rms amplitude Y of the case motion and the rms amplitudes Z_p and Z_c for the masses relative to the case are

$$Z_c = \frac{Y\Omega_c^2}{\sqrt{(1-\Omega_c^2)^2 + \frac{\Omega_c^2}{Q_c^2}}} \quad \text{and} \quad Z_p = \frac{Y\Omega_p^2}{\sqrt{(1-\Omega_p^2)^2 + \frac{\Omega_p^2}{Q_p^2}}} \tag{2}$$

where $\Omega_p = \omega/\omega_{op}$, $Q_p = m_p\omega_{op}/R_p$, $\Omega_c = \omega/\omega_{oc}$, and $Q_c = m_c\omega_{oc}/R_c$.

From the relative displacement $z \equiv z_c - z_p$ of the two independently-suspended masses, the rms amplitude of relative motion is

$$Z(rms) = \sqrt{Z_c^2 + Z_p^2 - 2Z_cZ_p\cos(\phi_c - \phi_p)} \tag{3}$$

where

$$\phi_c = \tan^{-1}\frac{\omega\omega_{oc}}{(\omega_{oc}^2 - \omega^2)Q_c} \quad \text{and} \quad \phi_p = \tan^{-1}\frac{\omega\omega_{op}}{(\omega_{op}^2 - \omega^2)Q_p} \tag{4}$$

The transfer function between the measured motion Z and the desired case motion Y is given by Eqns. 2-4. The frequency range of interest is $\omega << \omega_{oc}$, that is, frequencies less than the natural frequency of the cantilever. By design, the proof mass natural frequency is small compared to the cantilever natural frequency, so $\Omega_c << \Omega_p$ and, accordingly, $Z_c << Z_p$. Thus, in the band of interest, the **transfer function** is approximately

$$Z \approx \frac{Y\Omega_p^2}{\sqrt{(1-\Omega_p^2)^2 + \frac{\Omega_p^2}{Q_p^2}}} \quad . \tag{5}$$

The suspended masses are subject to thermal noise,[21] which may be included in the equation of motion as a force $F(rms) = \sqrt{4k_B T R}\ N/\sqrt{Hz}$; this is the Nyquist relation for a mass-spring oscillator with damping coefficient R. Thesteady-state solutions for thermal noise at frequency ω are oscillations with rms amplitudes

$$Z_{np} = \sqrt{\frac{4\,k_B\,T}{\omega_{op} k_p Q_p [(1-\Omega_p^2)^2 + \frac{\Omega_p^2}{Q_p^2}]}} \tag{6}$$

$$Z_{nc} = \sqrt{\frac{4\,k_B\,T}{\omega_{oc} k_c Q_c [(1-\Omega_c^2)^2 + \frac{\Omega_c^2}{Q_c^2}]}} .$$

Using Eq. 5, the *case-equivalent rms* noise terms are.

$$Y_{np} \approx \frac{1}{\omega^2}\sqrt{\frac{4\,k_B\,T\,\omega_{op}}{m_p\,Q_p}} \quad \text{and} \quad Y_{nc} \approx \frac{1}{\Omega_p^2}\sqrt{\frac{4\,k_B\,T[(1-\Omega_p^2)^2 + \frac{\Omega_p^2}{Q_p^2}]}{\omega_{oc}k_cQ_c\,[(1-\Omega_c^2)^2 + \frac{\Omega_c^2}{Q_c^2}]}} \quad (7)$$

where the subscripts c and p refer to parameters of the cantilever and the proof mass.

From the shot noise expression $I_n = \sqrt{2eI}$ Amps /~, coupled with the tunnel current relation, the case-equivalent shot noise in the tunnel current I is

$$Y_{ns} \approx \frac{1}{\Omega_p^2}\sqrt{\frac{2e}{I\Phi\alpha^2}}\sqrt{((1-\Omega_p^2)^2 + \frac{\Omega_p^2}{Q_p^2})} \quad (8)$$

where Φ and a were defined earlier for the tunnel tip. Johnson noise in the tunneling process arises from the zero-bias interchange of electrons across the gap, and is independent of bias. For a tunnel current of 1 nA at a tip bias of 100 mV, the case-equivalent Johnson noise is 0.7 times the shot noise given by Eq. 8. Johnson noise at the first resistor in the electronic circuit, typically 10 MCI, is a factor of 4 less than the tunnel current shot noise. Because of the large responsivity of the tunnel transducer, amplifier noise is unimportant. An important conclusion from Eq. 7 is that thermal noise equivalent case displacement for the proof mass is proportional to $\sqrt{f_o / mQ}$. Thermal noise equivalent acceleration of the case at frequency ω is readily obtained from the product of $0)^2$ and the noise equivalent case displacement.

Theoretical thermal noise equivalent case accelerations are shown in Fig. 4 for a 100 mg proof mass with a 100 Hz natural frequency and a 9 microgram cantilever with a 16 kHz natural frequency. A Q of 200 has been taken for both elements. Actual Q

values for silicon may be much higher. Shot noise is calculated for a tunnel current of 1 nA. As the figure shows, for these parameters, thermal noise in the proof mass dominates for a band of several hundred Hz. Thermal noise from the cantilever mass is comparable in magnitude to shot noise and Johnson noise and above several hundred Hz they dominate, increasing as f2. The noise equivalent acceleration of about 2X10-8 $g/\sqrt{Hz}$ illustrated in the figure corresponds to a proof mass relative motion of 5 x 10-4 Å, which tunneling transducers are capable of measuring.2 Thus, it can be concluded that it is possible to construct an accelerometer with a proof mass as small as 100 mg which can detect signals of the order of 10-9 $g/\sqrt{Hz}$. According to Eq. 8, the low frequency thermal noise can be reduced by increasing mQ/f_o; thus, larger mQ product and smaller f. can be utilized to improve performance. Q > 1 introduces a peak in the Z-displacement/case-acceleration transfer function at the proof mass resonance. If this peak is in the frequency band of interest, and particularly if Q is large, techniques to accommodate it may' be utilized, Such techniques include straightforward signal processing or utilization of a pair of detectors with different resonant frequencies for each axis of motion. Alternatively, for very large Q it may be suitable to block a narrow frequency band encompassing the peak.

This analysis also shows the difficulties encountered in fabricating sensitive accelerometers with extremely small proof masses in the microgram range. For example, for a proof mass of 1 microgram and a Q of 1000, the thermal noise equivalent acceleration from Eq. 7 is 3 x 10-6 $g/\sqrt{Hz}$ for a natural frequency of 10 kHz, and 10-5 $g/\sqrt{Hz}$ for a natural frequency of 100 kHz, several orders of magnitude larger than the 2 x 10-9 $g/\sqrt{Hz}$ illustrated in Fig. 4.

EXPERIMENTAL

We have constructed and tested prototype dual-element accelerometers of micromachined silicon with 50 to 260 mg proof masses. The 260 mg mass includes a tungsten metal element bonded to the silicon, As illustrated schematically in Fig. 1, the proof mass is suspended from a silicon spring on one end. The high-frequency cantilever is 4 microns thick and 0.7 mm long, and is comprised of boron-doped Ge-alloyed silicon. Ge alloying is chosen to compensate for the heavy boron doping in order to give a low-stress cantilever. External chip dimensions are 13 mm x 13 mm. A silicon tip is formed directly on the silicon proof mass, by undercutting a 60x60 micron square of Si02 with ethylenediamine pyrocatechol (EDP) etchant until the fragment of oxide is carried away, leaving a pyramidal tip. A photomicrograph of a gold-coated silicon tip is shown in Fig. 5.

Tests have been conducted in air and in vacuum. Vibration tests were conducted with the test device and a calibrated Kistler Model K-Beam accelerometer mounted in proximity on a massive metal plate. This massive plate was suspended from a tripod with elastic cords to provide isolation from floor vibration. The plate was excited sinusoidally, and signals from both accelerometers were measured on a Hewlett-Packard Model 3582A spectrum analyzer. The silicon mass chip was suspended vertically, and the mounting plate was vibrated horizontally. Results of measurements in a partial vacuum of about 100 T are shown in Fig. 6, where the responsivity in Volts/g is plotted from 4 to 600 Hz. At low frequency the responsivity is approximately 105 V/g, decreasing to about 1300 V/g at 600 Hz. The measured noise level is 10-7 $g/\sqrt{Hz}$ from 4 to 70 Hz and 6 x 10-7 $g/\sqrt{Hz}$ at 400 Hz, This noise level is believed to be due to environmental acoustic sources and not a limit of the device. The device is heavily damped by the air squeeze film between the proof mass deflection electrodes, as evidenced from the small slope in Fig. 6 relative to the $1/f^2$ falloff expected above the

resonant frequency for low darnping. A $1/f^2$ dependence above 50 Hz has been observed for this device in a vacuum of 1 T. The signal from the tunnel accelerometer is within 1% of linear over a 70 dB dynamic range, as expected, given the design of the suspension and the nature of the force rebalance mode of operation. Linearity of another prototype with a 50 mg proof mass measured at atmospheric pressure and 100 Hz is shown in Fig. 7.

Devices have been fabricated both with and without shaped silicon tips of the form illustrated in Fig. 5, Similar data, including that of Fig. 7, are obtained from a, device with no protruding tip of that form, relying on the fact that tunneling will take place between the nearest atoms, so that a sharp tip is not essential. In this case the high-frequency cantilever is triangular in order to limit the region of nearest approach for tunneling. .

CONCLUSION "

Electron tunneling displacement transducers offer extremely high resolutions which can be utilized for sensitive microinstruments. A new dual-element micromachined silicon tunnel accelerometer which extends the operational bandwidth beyond the resonant frequency of the proof mass has been successfully fabricated and demonstrated. The dual-element design, comprising a low-resonant-frequency proof mass oscillator and a high-frequency tunnel transducer cantilever, provides flexibility for independently optimizing the proof mass oscillator and the tunnel transducer. In a heavily damped system with $Q<<1$, the responsivity is large, being 1 V for a 10-5 g acceleration at 10 Hz. The noise floor for the same system is 10-7 $g/\sqrt{Hz}$ at 4 to 70 Hz and 6 x 10-7 $g/\sqrt{Hz}$ at 400 Hz.

Thermal noise analysis is essential for microaccelerometers with small proof masses. Analysis for a system with a 100 mg proof mass and a proof mass resonant

frequency of 100 Hz shows that the. dominant noise source is thermal noise of the suspended masses. Electronic noise for an electron tunnel transducer is less. This noise anal ysis shows that compact accelerometers with proof masses in the range of 100 mg are capable of measuring signals significantly less than 1()-~ g; Qs greater than 1 are necessary to sense nano-g signals. For a 100 mg proof mass, a 100 Hz resonant frequency, and a Q of 200, an acceleration resolution approaching 1()-~ $g/\sqrt{Hz}$ in a 300 Hz band and 10^{-8} $g/\sqrt{Hz}$ at 1 kHz are predicted for the dual-element device. Electron tunnel sensors are necessary for these high resolutions in small devices with this magnitude of proof mass.

ACKNOWLEDGMENTS

The research described in this paper was performed by the Center for Space Microelectronics Technology, Jet Propulsion Laboratory, California Institute of Technology, and was jointly sponsored by Naval Air Warfare Center, Ballistic Missile Defense Organizjation/innovative. Science and Technology Office, and Advanced Research Projects Agency, through an agreement with the National Aeronautics and Space Administration.

REFERENCES

1 S. B. Waltman and W. J. Kaiser, An electron tunneling sensor, *Sensors and Actuators, 19 (1989) 201-210.*

2 T. W. Kenny, S. B. Waltman, J. K. Reynolds, and W. J, Kaiser, A micromachined silicon electron tunneling sensor, *Proc. IEEE Micro Electro Mechanical Systems Conference, Napa Valley, U.S.A, 1990,* pp. *192-196;* ibid., *Micromachined silicon tunnel sensor for motion detection, Appl. Phys. Letters, 58 (1991)* 100-102.

3 A, A. Baski, T. R. Albrecht, and C. F. Quate, *Tunneling accelerometer, J. Microscopy, 157 (1988) 73-76.*

4 T. W. Kenny, W. J. Kaiser, J. K. Reynolds, J. A. Podosek, H. K. Rockstad, E. C. Vote, and S. B. Waltman, *Electron tunnel sensors, J. Vat. Sci. Technol., AIO (1992) 2114-2118.*

5 J. J. Yao, S. C. Arney, and N. C. MacDonald, Fabrication of high-frequency two-dimensional nanoactuators for scanned probe devices, *J. MicroElectroMechanical Systems 1 (1992) 14-22.*

6 D. Kobayashi, T. Hirano, T. Furuhata, and H. Fujita, An integrated lateral tunneling unit, *Proc. Micro Electro Mechanical Systems, Travemunde, Germany, 1992,* pp. *214-219,*

7 P. M. Zavracky, F. Hartley, N. Sherman, T. Hansen, and K. Warner, A new force balanced accelerometer using tunneling tip position sensing, *Abs. Lute News Papers, 7th Int. Conf. Solid-State Sensors and Actuators (Transducers '93), Yokohama, Japan, June 7-10, 1993,* pp. 50-51.

8 J. H. Wandass, J. S. Murday, and R. J. Colton, *Magnetic field sensing with magnetostrictive materials using a tunneling tip detector, Sensors and Actuators, 19 (1989) 211-225.*

9 R. A. Brizzolara, R. J. Colton, M. Wun-Fogle, and H. T. Savage, A *tunneling tip magnetometer, Sensors and Actuators, 20* (1989)199-205.

10 T. W. Kenny, W, J. Kaiser, S. B. Waltman, and J. K. Reynolds, *Novel infrared sensor based on a tunneling displacement transducer, Appl. Phys. Letters 59* (1991) *1820-1822.*

11 J. C. Jiang and R. C. White, Fabrication of micromachined silicon tip transducer for tactile sensing, *J. Vat. Sci. Technol.*, to be published, August (1993).

12 M. F. Bocko, K. A. Stephenson, and R. H. Koch, *Vacuum tunneling probe: a nonreciprocal, reduced-back-action transducer, Phys. Rev. Letters 61 (1988) 726-729.*

13 B. Yurke and G. P. Kochanski, *Momentum noise in vacuum tunneling transducers, Phys. Rev. B41 (1990) 8184-8194.*

14 G. Binnig and H. Rohrer, *Scanning tunneling microscopy, IBM J. Res. Develop. 30* (1986) 355-369.

15 W. D. Frobenius, S. A. Zeitman, M. H. White, D. D. O'Sullivan, and R. G. Hamel, *Microminiature ganged threshold accelerometers compatible with integrated circuit technology, IEEE Trans. Elect. Devices, ED-19 (1972) 37-40.*

16 L. M. Roylance and J. B. Angell, *A batch-fabricated silicon accelerometer, ibid., ED-26 (1979) 1911-1917.*

17 K. E. Petersen, A. Shartel, and N. F. Raley, *Micromechanical accelerometer integrated with MOS detection circuitry, " ibid., ED-29(1982) 23-27.*

18 F. Rudolph, *Precision accelerometers with μ g resolution, Sensors and Actuators, A21-A23 (1990) 297-281.*

19 D. W. de Bruin, H. V. Allen, S, C. Terry, *Second-order effects in self-testable accelerometers, Tech. Digest, IEEE Solid-State Sensor and Actuator Workshop, Hilton Head Island, SC, U, S.A., June 22-2S, 1990*, pp. 149-152.

20 W. Henrion, L. DiSanza, M. Ip, S. Terry, and H, Jerman, *Wide dynamic range direct digital accelerometer, ibid.,* 153-157.

21 T. B. Gabrielson, *Mechanical-thermal noise in micromachined acoustic and vibration sensors, IEEE Trans. Electron Devices, 40 (1993)* 903-909.

FIGURE CAPTIONS

Figure 1. Schematic illustration of a micromachined dual-element electron tunneling accelerometer. The boron-doped epitaxial silicon layer is used for the wide-bandwidth cantilever.

Figure 2. Tunnel transducer feedback circuitry.

Figure 3, Schematic illustration of a two-mass system with spring constants k_p and k_c and damping coefficients R_p and R_c for the proof mass and the wide-bandwidth cantilever.

Figure 4. Thermal noise equivalent case acceleration for various noise sources including thermal vibration of two masses and shot noise in the electron tunneling current.

Figure 5. An SEM photomicrograph of a micromachined silicon tip, after application of a gold coating.

Figure 6. Tunnel accelerometer responsivity vs. frequency, for a device having a proof mass of 260 mg, measured in a pressure of approximately 100 Torr.

Figure 7. Linearity of the tunnel accelerometer output with respect to a reference accelerometer, for a tunnel device having a proof mass of 50 mg measured at 100 Hz in 1 atmosphere.

FIGURE CAPTIONS

Figure 1. Schematic illustration of a micromachined dual-element electron tunneling accelerometer. The boron-doped epitaxial silicon layer is used for the wide-bandwidth cantilever.

Figure 2. Tunnel transducer feedback circuitry.

Figure 3. Schematic illustration of a two-mass system with spring constants k_p and k_c and damping coefficients R_p and R_c for the proof mass and the wide-bandwidth cantilever.

Figure 4. Thermal noise equivalent case acceleration for various noise sources including thermal vibration of two masses and shot noise in the electron tunneling current.

Figure 5. An SEM photomicrograph of a micromachined silicon tip, after application of a gold coating,

Figure 6. Tunnel accelerometer responsivity vs. frequency, for a device having a proof mass of 260 mg, measured in a pressure of approximately 100 Torr.

Figure 7. Linearity of the tunnel accelerometer output with respect to a reference accelerometer, for a tunnel device having a proof mass of 50 mg measured at 100 Hz in 1 atmosphere.

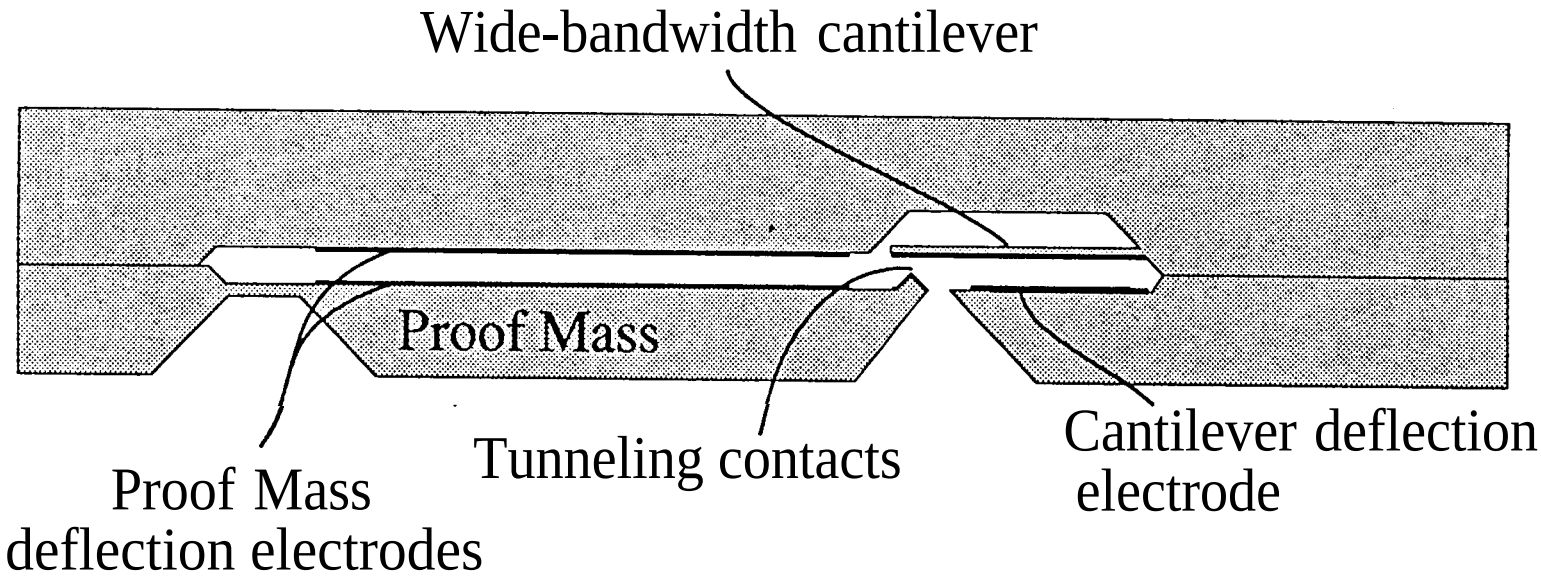
Wide-bandwidth cantilever
Proof Mass
Proof Mass
deflection electrodes
Tunneling contacts
Cantilever deflection
electrode

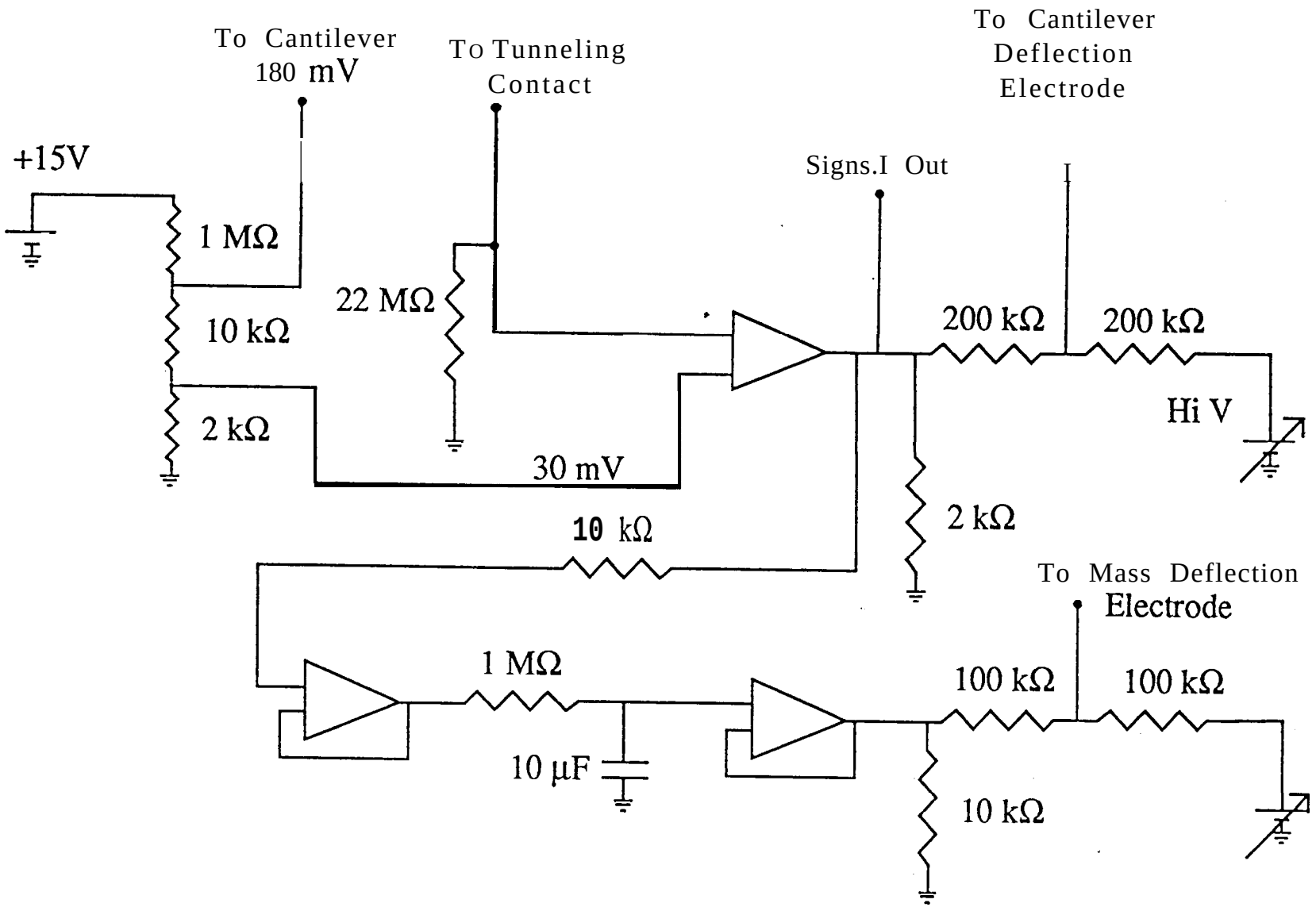
To Cantilever
180 mV
To Tunneling
Contact
To Cantilever
Deflection
Electrode
+15V
Signs.I Out
1 MΩ
22 MΩ
10 kΩ
200 kΩ
200 kΩ
2 kΩ
Hi V
30 mV
2 kΩ
10 kΩ
To Mass Deflection
Electrode
1 MΩ
100 kΩ
100 kΩ
10 µF
10 kΩ

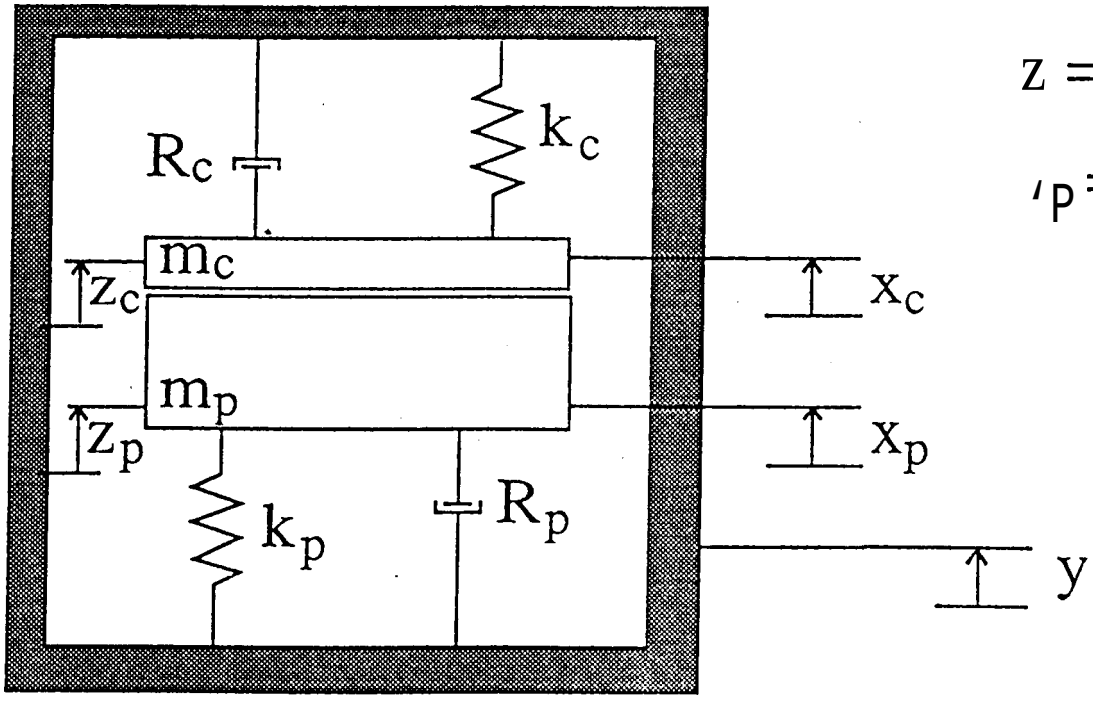

$z = z_c - z_p$

$'_p = x_p - y$

Case

ROCKSTAD
FIG. 3

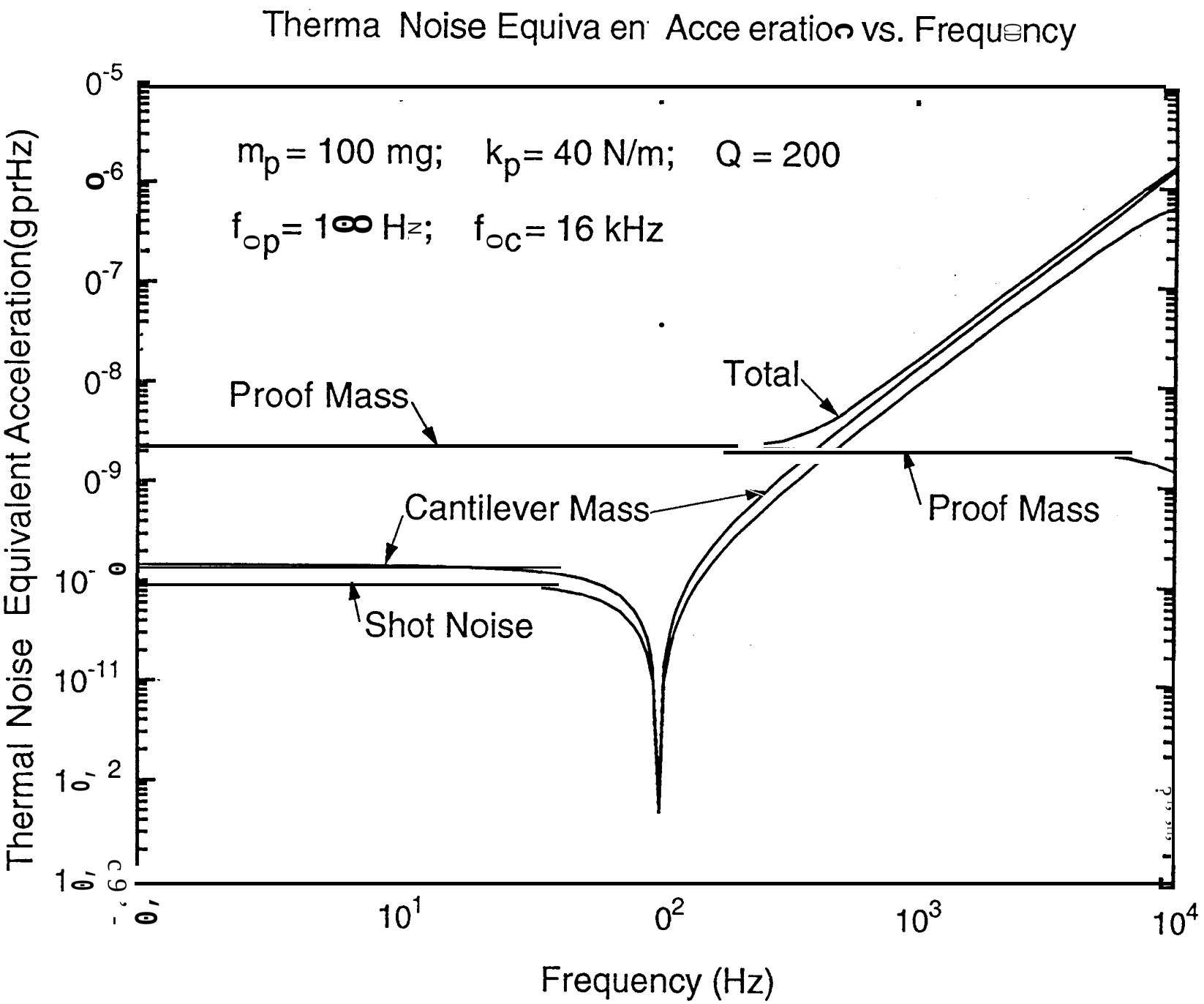
Therma Noise Equiva en Acce eratio vs. Frequ ncy
m_p = 100 mg; k_p = 40 N/m; Q = 200
f_{op} = 1 Hz; f_{oc} = 16 kHz
Proof Mass
Total
Cantilever Mass
Proof Mass
Shot Noise
Thermal Noise Equivalent Acceleration(g prHz)
Frequency (Hz)
10^{1}
10^{3}
10^{4}

0000 20KV X400

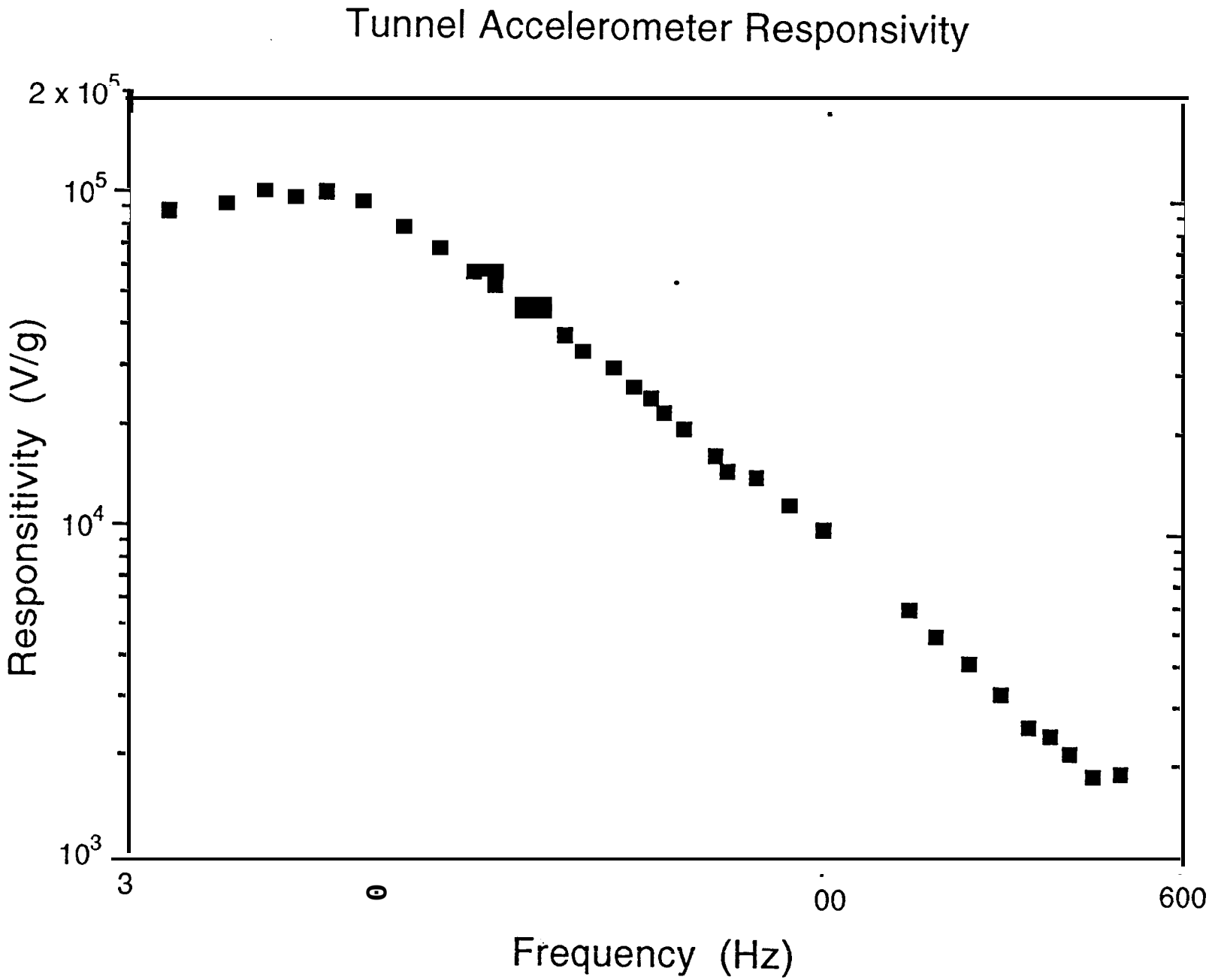
Tunnel Accelerometer Responsivity
2 x 10^5
10^5
10^4
10^3
Responsitivity (V/g)
3
0
00
600
Frequency (Hz)

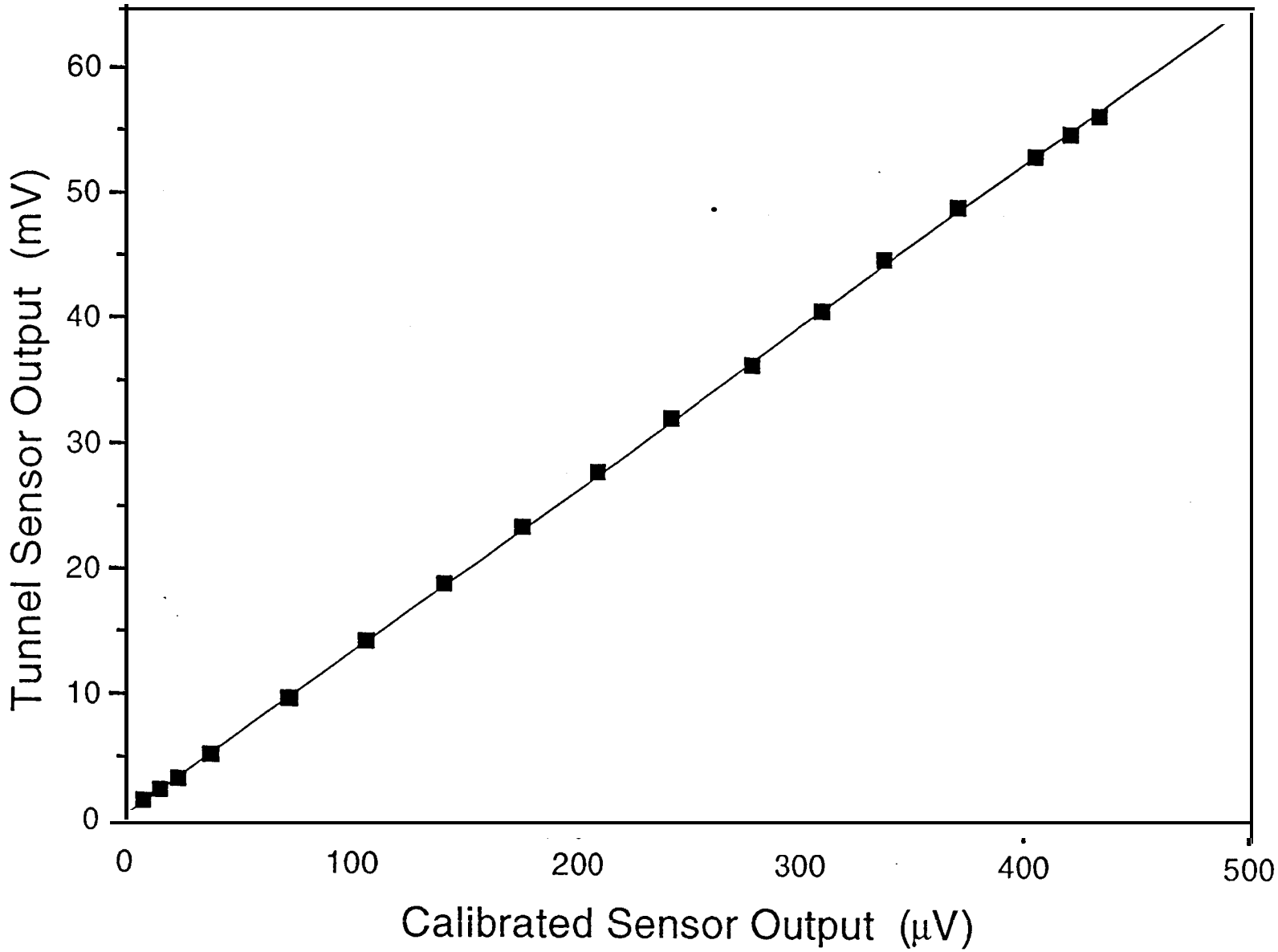
Tunnel Sensor Output (mV)
0
10
20
30
40
50
60
0
100
200
300
400
500
Calibrated Sensor Output (μV)